Article

Probing the Surface of Noble Metals Electrochemically by Underpotential Deposition of Transition Metals

Nolwenn Mayet, Karine Servat, K. Boniface Kokoh and **Teko W. Napporn** *

IC2MP, UMR 7285 CNRS, Université de Poitiers, 4 rue Michel Brunet B27 TSA 51106, 86073 Poitiers CEDEX 09, France; nolwenn.mayet@univ-poitiers.fr (N.M.); karine.servat@univ-poitiers.fr (K.S.); boniface.kokoh@univ-poitiers.fr (K.B.K.)

* Correspondence: teko.napporn@univ-poitiers.fr

Abstract: The advances in material science have led to the development of novel and various materials as nanoparticles or thin films. Underpotential deposition (*upd*) of transition metals appears to be a very sensitive method for probing the surfaces of noble metals, which is a parameter that has an important effect on the activity in heterogeneous catalysis. Underpotential deposition as a surface characterization tool permits researchers to precisely determine the crystallographic orientations of nanoparticles or the real surface area of various surfaces. Among all the work dealing with *upd*, this review focuses specifically on the main *upd* systems used to probe surfaces of noble metals in electrocatalysis, from poly- and single-crystalline surfaces to nanoparticles. Cu_{upd} is reported as a tool to determine the active surface area of gold- and platinum-based bimetallic electrode materials. Pb_{upd} is the most used system to assess the crystallographic orientations on nanoparticles' surface. In the case of platinum, Bi and Ge adsorptions are singled out for probing (1 1 1) and (1 0 0) facets, respectively.

Keywords: underpotential deposition (*upd*); Au; Pt; Pd; nanoparticles; cyclic voltammetry; electrocatalysis

1. Introduction

Surface of materials is a key parameter in heterogeneous catalysis. Moreover, in electrocatalysis, it is the reaction site where the exchange of electrons occurs, thereby the structure of the materials or any roughness affect their electrochemical response. Referring the current density to the geometric surface area does not consider the surface structure of the material, however, the active sites at the surface of a material depend on its structure, therefore, the characterization of material surface in electrocatalysis becomes an important step in understanding the reactions that occur and evaluating their activity. Several electrochemical methods are used for characterizing the material surface. The underpotential deposition (*upd*) appears to be a powerful tool for probing the surface of electrocatalysts. The *upd* is sensitive to local order, contrary to electron diffraction methods such as Low Energy Electron Diffraction (LEED) or Reflexion High Energy Electron Diffraction (RHEED) which are more sensitive to long-range order [1]. The *upd* can be carried out on polycrystalline surfaces, single-crystals, and recently nanoparticles. The latter have different shapes and sizes that involve different surface structures leading to a variety of activities observed in heterogeneous catalysis and in electrocatalysis. The development of nanoscaled materials in electrochemistry implies the increase of the utilization of *upd* for various applications, from surface probing to the synthesis of nanomaterials.

2. Generalities about *upd*

2.1. Principles and Thermodynamics of the upd Process

The *upd* of a metal is defined as the deposition of a metal onto a foreign metallic substrate in a potential region where a new and pure phase does not form on the substrate.

Figure 1 shows a schematic representation of the voltammetric profile for *upd* and the overpotential deposition (*opd*) of a metal on a foreign substrate. The *upd* occurs at higher potentials than the potential of reduction ($E_{upd} > E$) because of the strong interactions between the deposited metal and the substrate surface structure. In the *upd* region, the metal is deposited as a monolayer on the substrate through self-limiting deposition. In the *opd* region, the metal is deposited as multilayers (bulk electrodeposition) in the absence of self-limiting behavior, creating rough structures [2].
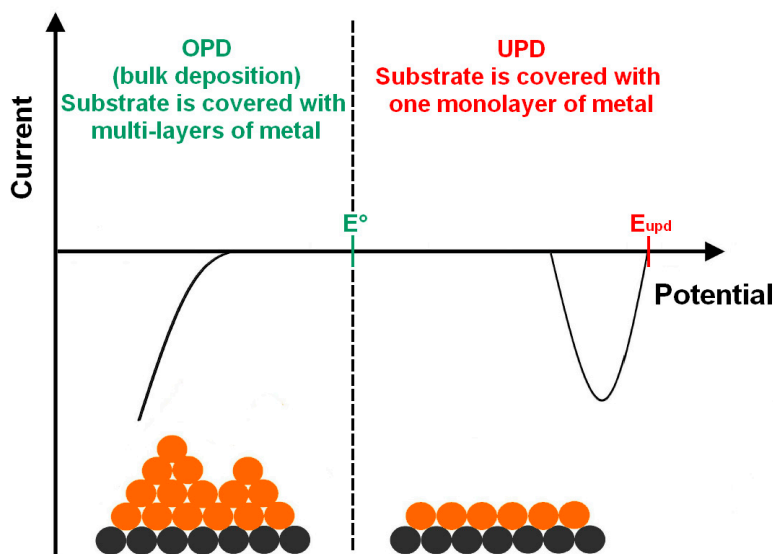
Figure 1. Schematic profile of a voltammetric curve showing the underpotential deposition (*upd*) and overpotential deposition (*opd*) processes of a metal (in orange) on a foreign substrate (in black).

The reduction potential E_{eq} of the metal (M) associated with the reaction $M^{n+} + ne^- \rightarrow M$ is determined by the Nernst equation:

$$E_{eq} = E^\circ + \frac{RT}{nF} ln \frac{a_{Mn+}}{a_M},\tag{1}$$

where E_{eq} is the Nernst potential of the reaction, E° is the standard potential of the reaction, R is the universal gas constant, T is the temperature, n is the number of exchanged electrons in the reaction, F is the Faraday constant, a_{Mn+} is the activity of M^{n+} ions, and a_M is the activity of the condensed phase M ($a_M = 1$).

The difference between the *upd* onset potential (E_{upd}) and the bulk electrodeposition potential (E) is correlated to the work function of the deposited metal and the substrate [3]. The underpotential shift ($\Delta U = E_{upd} - E$) can be plotted against the difference in work function between bulk substrate and bulk deposited metal $\Delta\Phi$ [3]:

$$\Delta U = \alpha\Delta\Phi, \alpha = 0.5 \text{ V eV}^{-1}.\tag{2}$$

This linear relation between underpotential shift and work function difference suggests that the covalent part of the ad-atom-substrate bond does not differ appreciably to the bond strength between the ad-atom and the surface of the same metal.

The thermodynamic aspects of *upd* has been extensively reported on both polycrystalline and single-crystalline surfaces [4–6]. It shows clearly that the interaction between particle and substrate has a strong effect on the changes in work function and also the interaction between particles, which leads to several energy states. The effect of partially charged *upd* species that leads to the absence of discreteness of charge has been also reported [6]. The theoretical aspect of *upd* has been reported to understand thermodynamics behind this phenomenon [7,8]. It is well known that crystallographic orientation, defects (steps, kinks, grain boundaries), surface reconstruction [9], and alloying play a crucial role in the initial steps of metal deposition. Figure 2 shows the three low Miller indices for a faces-centered cubic (*fcc*) system. The plane (1 1 1) is the most compact arrangement by comparison to the more opened (1 1 0) plane.

(1 1 1)   **(1 0 0)**   **(1 1 0)**
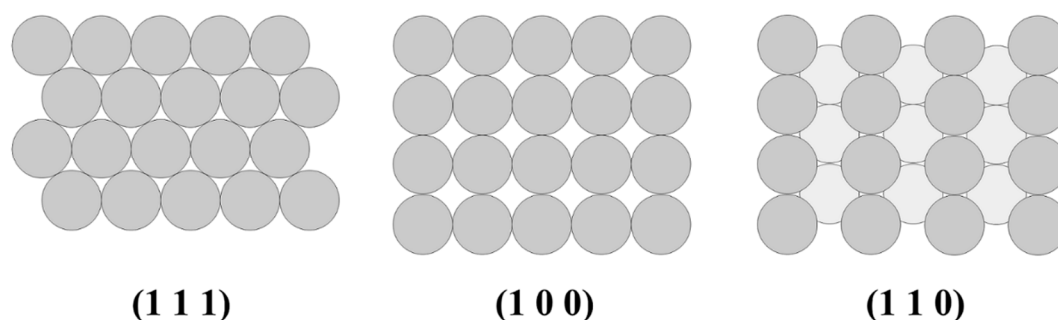
Figure 2. Representation of the three low Miller indices for a faces-centered cubic system.

2.2. A Method of Characterization: Cyclic Voltammetry

Different techniques can be employed to characterize *upd* layers [10]. Cyclic voltammetry is the method most used for carrying out the *upd* of a metal over a substrate. It consists in linearly applying a potential with a constant scan rate *(dE/dt)* on the electrode, between two fixed potential limits. The current is monitored during the scans, the current-potential curves (voltammograms) show the oxidation-reduction processes that occur at the surface. The *upd* curves display cathodic and anodic peaks, for the deposition and dissolution of the deposited metal, respectively. The presence of several distinct adsorption peaks on the voltammograms indicates that the formation of the monolayer takes place at different energetic adsorption steps. The structure of the peak strongly depends on the crystallographic orientation of the substrate and the defects. The peaks are not well defined for polycrystalline electrodes, which present different crystallographic orientations and a high density of defects (kinks, grain boundaries, steps, etc.)—by comparison with single-crystal electrodes.

2.3. The upd Metals

Various substrates were used to perform the *upd* of a metal. The studies began with polycrystalline substrates [11,12], which have a mixed surface structure. To understand and explain the phenomenon, well defined surfaces are proposed. Therefore, *upd* of a metal monolayer onto polycrystalline or single-crystal substrates of a foreign metal has been studied intensively. These investigations included various substrates such as Au, Pt, Ag, Cu, Rh, Ru, Pd, and many deposited ions like Ag^+ [13,14], Cu^{2+} [15–24], Cd^{2+} [25], Pb^{2+} [26–30], Tl^+ [31–34], Cd^{2+} [35,36], Hg^{2+} [37], Sn^{2+} [38,39], Bi^{3+} [30,40–45], Ge^{4+} [46–48], Sb^{2+} [49–51], and Ni^{2+} [52]. The charge corresponding to the *upd* permits researchers to estimate the amount of deposited metal. It is assumed that the metal ions in the sub-monolayers are completely discharged, even if partially charged deposits have been reported. In a large number of studies, the effect of a foreign metal monolayer deposited by *upd* on a metallic substrate was investigated in relation to electrocatalytic reactions [53,54]. Indeed, the *upd* of a monolayer of a foreign metal on a substrate modifies its surface structure. This modification has the advantage of affecting the adsorbed species on the surface and thus the electrochemical reaction. The metal deposited

is called ad-atom. It was used in electrosynthesis to modulate the fabrication of different reaction products from the same compound [55,56]. The *upd* process also plays a crucial role in the synthesis of nanoparticles. The layer obtained by *upd* can be the precursor for fabricating nanoparticles of noble metals by galvanic replacement [57]. In this short review, *upd* of transition elements on noble metals' surfaces will be addressed. It includes how surface crystallographic orientations are probing and describes the determination of electrochemically active surface area (ECSA).

3. The M$_{upd}$ on Noble Metals: Au, Pt, and Pd

3.1. The Case of Au

3.1.1. Cu on Au

The underpotential deposition of Cu (Cu$_{upd}$) on low-index facets of Au appears to be the most extensively studied system. A large number of studies concerns the Cu$_{upd}$ on gold single-crystal Au(1 1 1) [16,18,20,23,58–65]. Investigations on the electrode surface permitted to provide evidences of the Cu$_{upd}$ species at the strained gold surface [24,66]. It is difficult to calculate the *upd* shift of copper ions using electrolytes containing different anions because of their effect. Indeed, anions provide a great influence on the Cu$_{upd}$ on Au, leading to different surface structures and onset potentials of the *upd* process [21,22,67,68]. Cu$_{upd}$ has been investigated on different gold surface orientations (low and high index). Therefore, Cu$_{upd}$ on Au(1 0 0) has been scrutinized by scanning tunneling microscopy (STM) in hydrochloric and sulfuric acids. A (1 × 1) copper ad-layer structure was reported in sulfuric acid, while an incommensurate (2 × 1) one-dimensional structure was observed when hydrochloric acid was added [59]. These anions are specifically adsorbate species because chloride anions are more strongly bound on the gold surface than sulfate anions. Moreover, in the presence of bromide anions on Au(1 1 1) and Pt(1 1 1), a study realized has demonstrated once again that the anions have an influence on the *upd* process and the stability of the deposited ad-layer [17]. It also strongly depends on the substrate because the different behaviors on Cu$_{upd}$ originate from geometric constraint imposed by the lattice structure relative to the deposited ad-layer rather than from energetic considerations. The studies of Cu$_{upd}$ on Au(1 1 1) in sulfuric acid media suggest the co-adsorption of 2/3 monolayer of copper and 1/3 of sulfate (SO$_4^{2-}$) [15]. This gives a pseudomorphic ($\sqrt{3} \times \sqrt{3}$) structure, followed by a further deposition of 1/3 monolayer of copper and completion of a full epitaxial (1 × 1) monolayer of copper which is still covered by a ($\sqrt{3} \times \sqrt{3}$) layer of sulfate anions [18]. A recent study goes further into the mechanism of Cu$_{upd}$ in the presence of sulfates [21,22]. Indeed, cyclic voltammetry investigations were performed on Au(1 1 1) in both *upd* and *opd* regions. In the potential region where the Cu$_{upd}$ takes place, the first peaks which correspond to the phase transition of sulfate anions on Au(1 1 1) substrate were observed. During the cathodic potential sweep, the adsorption of 2/3 monolayer and then 1/3 monolayer of copper, both with the co-adsorption of sulfate anions, were respectively obtained. During the anodic potential sweep, desorption of the formed monolayer occurs. When the CV is recorded in both *upd* and *opd* regions at lower potentials, the process of adsorption/desorption of multilayer copper is observed. According to these authors, the EC-STM images reveal the nucleation of the ($\sqrt{3} \times \sqrt{7}$) sulfate structure. At −500 mV vs. Pt/PtO, the ($\sqrt{3} \times \sqrt{3}$) structure of SO$_4^{2-}$ anions on 2/3 ML of copper can be seen on HR-STM image. This structure is also observed on two-dimensional gold islands. These islands are provided from the lifting of the (1 1 1) reconstruction. This study shows that different structures are observed on terraces resulting from different local thickness of copper. A ($\sqrt{3} \times \sqrt{3}$)-like structure of sulfate is typical of an incomplete second layer of copper. Figure 3 shows a model (top view) of the sulfate structure ($\sqrt{3} \times \sqrt{3}$), and 2/3 of monolayer of Cu, and the sulfate structure ($\sqrt{3} \times \sqrt{7}$) on the first pseudomorphic monolayer of Cu deposited on Au (1 1 1).
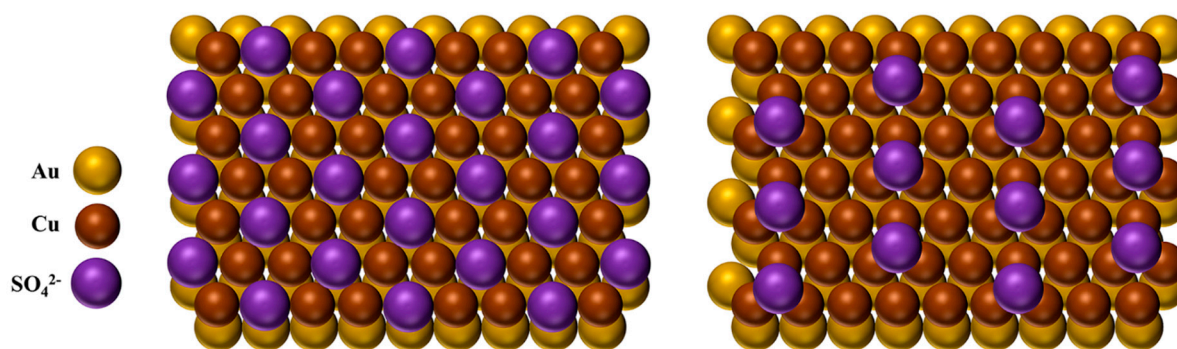
Figure 3. Model of the ($\sqrt{3} \times \sqrt{3}$) sulfate structure, with 2/3 of Cu monolayer (left) and ($\sqrt{3} \times \sqrt{7}$) sulfate structure on the first pseudomorphic monolayer of Cu underpotentially deposited (right) on Au (1 1 1).

Cu_{upd} studies were carried on stepped surfaces of gold with [(n−1)(1 1 1) × (1 1 0)] (n = 6, 7, 10) structures [19]. Figure 4 shows the voltammograms for Cu_{upd} on (3 3 2), (7 7 5), and (5 5 4) surfaces of Au. These structures are made of (1 1 1) terraces and (1 1 0) steps. The voltammogram of Au(3 3 2) displays two broad and overlapping peaks in the first adsorption/desorption region (at 0.520 and 0.560 V vs. RHE). When the step density decreases (the width n of the terrace increases), the peak at 0.560 V vs. RHE is decreasing and leads to assign it to (1 1 0) steps. This potential is close to the main *upd* peak on the Au(1 1 0) electrode (0.570 V vs. RHE). In the case of the peak at 0.520 V vs. RHE, the comparison with copper *upd* on Au(1 1 1) indicates the formation of ($\sqrt{3} \times \sqrt{3}$) R30° structure on the (1 1 1) terraces. It can be seen that this peak becomes better defined when the width of (1 1 1) terraces increases. By deconvoluting these peaks with Gaussian functions, it is found that the charge calculated for (1 1 0) steps on Au(3 3 2) is 17%, with respect to the total *upd* charge. By comparison, the relative geometric area of the (1 1 0) steps domain covers 16.7 % of the surface, which is in good agreement with the relative calculated charge. However, since Cu_{upd} is a complex function of sulfate coverage, it should be noticed that there is no significant change in the sulfate coverage in this potential range. It is necessary to measure the charge of the co-adsorbed sulfate anions in order to perform a full quantitative analysis of the copper *upd* charge on stepped surfaces. On the other hand, the voltammograms in Figure 4 display peaks between 0.350 V and 0.400 V vs. RHE. These peaks are attributed to the ($\sqrt{3} \times \sqrt{3}$) R30° → (1 × 1) phase transition on the (1 1 1) terraces. The splitting of this peak is also influenced by the step density but can be a consequence of the reconstruction of stepped surfaces. This study clearly shows that the steps have an influence on the energetic/kinetics of phase transition. It has been suggested that this influence could be either electronic or structural (Smoluchowski effect).
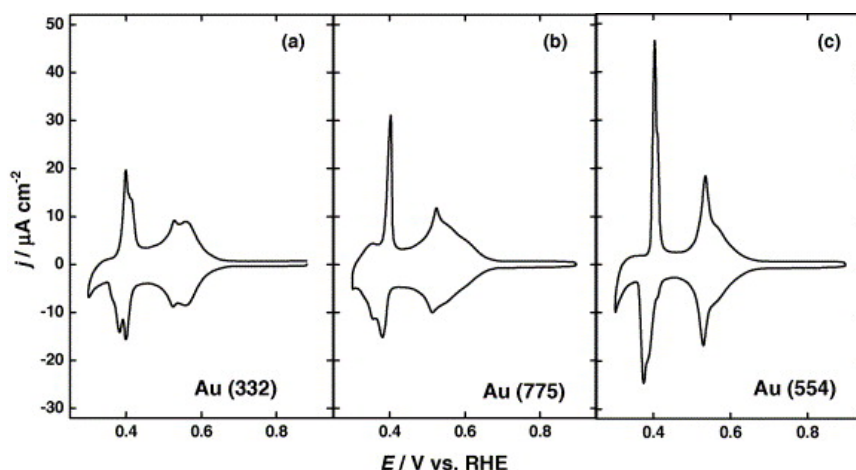
Figure 4. Cyclic voltammograms of (**a**) Au(3 3 2); (**b**) Au(7 7 5); and (**c**) Au(5 5 4) in 0.05 mol L^{-1} H$_2$SO$_4$ + 1 mmol L^{-1} CuSO$_4$ at 5 mVs^{-1}. Reprinted from reference [19]. Copyright (2004) with permission from Elsevier.

The Cu$_{upd}$ can be employed to quantify the surface area of nanoporous gold films [69]. The values obtained by this method are in agreement with those obtained by integrating the reduction peak of gold oxides. However, it should be noted that nanoporous gold films contain residual silver since their preparation consists of the dealloying of bimetallic films. The presence of silver can influence the Cu$_{upd}$, since this process does not occur on silver.

Many papers reported the effect of metal *upd* on the electrocatalytic activity of a material. In some cases, the underpotential deposited metal can inhibit or even totally deactivate the surface towards electrocatalytic reactions. Cu$_{upd}$ has been used in order to elucidate the mechanism of hydrogen evolution reaction on palladium-modified stepped gold surfaces [70]. The Cu$_{upd}$ allows us to block (deactivate) the palladium step sites towards hydrogen evolution reaction, which is not favored in the presence of copper. Figure 5 shows ball models for Au(h k l)/Pd surface, with steps blocked by copper ad-atoms.
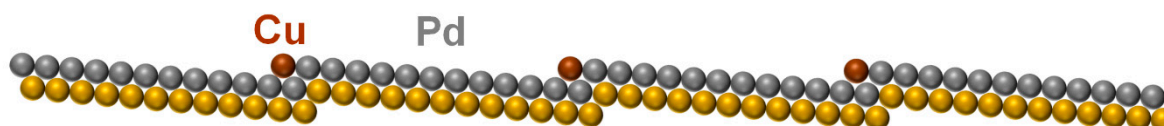
Figure 5. Ball models of Au(h k, l)/Pd (h = k, l =k−1) surface where the Pd steps sites are blocked by Cu modified with 1 ML of Pd.

A technique named Dynamic Electro-Chemo-Mechanical Analysis (DECMA) has been developed, which permits assessment of the strain effect on the adsorption process during Cu$_{upd}$ [24].

3.1.2. Pb on Au

Many studies of the surface structure of gold electrodes have been carried out through the *upd* of lead (Pb$_{upd}$). These studies allow us to assign the different voltammetric peaks of different surfaces to the deposition processes that occur on low index planes or terraces and steps. The influence of the crystallographic orientation on the process has been largely discussed [28]. Indeed, Pb$_{upd}$ has been reported on polycrystalline gold [71], low-index facets, on (1 0 0), (1 1 1), and vicinal facets [43,72], as well as a large variety of stepped surfaces [73].

Lead and gold atoms have very different sizes (lead is about 20% larger than gold), which favor the formation of incommensurate ad-layers. Indeed, the analysis of the structure of a lead monolayer

on Au(1 1 1) by X-ray diffraction shows a hexagonal structure [29]. Figure 6 shows a schematic representation of the structure of a lead monolayer on Au(1 1 1).
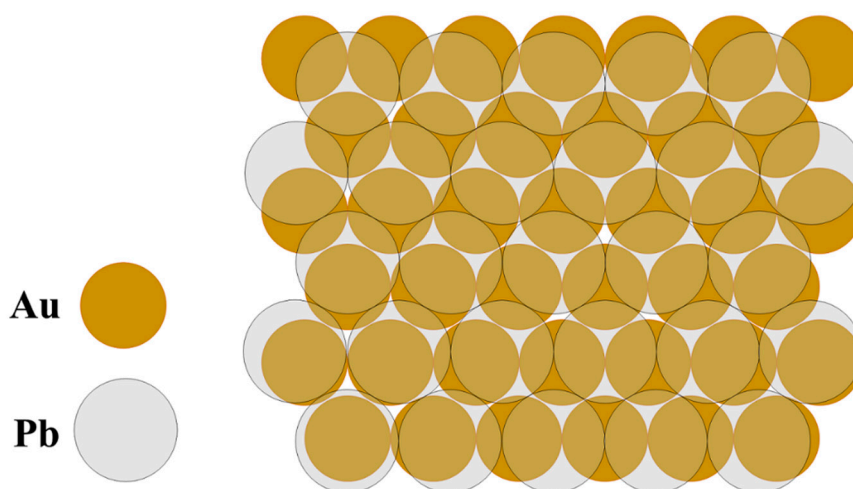
Au

Pb

Figure 6. Representation of the hexagonal monolayer of lead on Au(1 1 1).

One of the interesting features of Pb_{upd} on gold is the specific adsorption at different potentials depending on the surface orientation, as illustrated on a polycrystalline gold electrode (Figure 7). During the negative potential sweep (from high to low potentials), lead is deposited on (1 1 0) facets in the potential range from 0.55 to 0.47 V vs. RHE. The deposition on (1 0 0) facets occurs at around 0.43 V vs. RHE and at 0.38 V vs. RHE on (1 1 1). The peak profile (width, shift) depends on the domain width or the presence of terraces. This feature permits assessing the coverage of lead on various facets of gold and also the percentage of each facet on this surface [74].
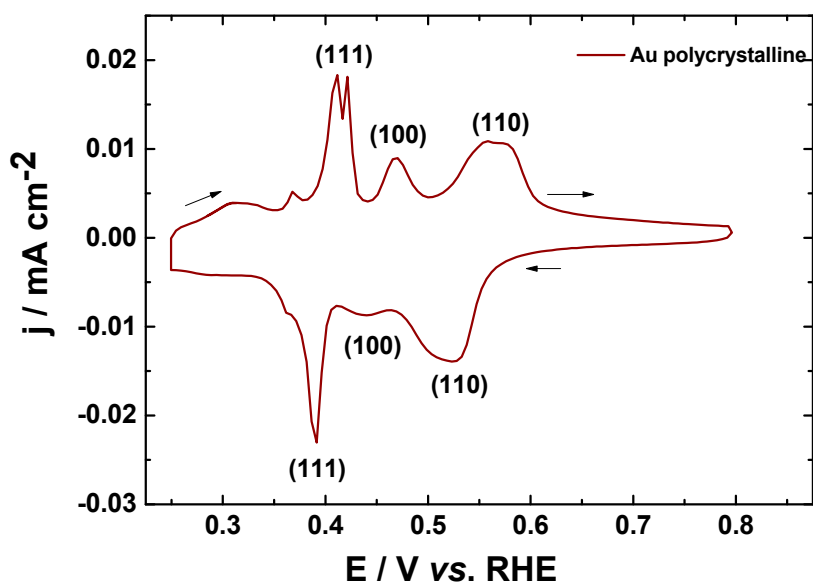
Figure 7. Cyclic voltammogram of Au polycrystalline in 0.1 mol L^{-1} NaOH + 1 mmol L^{-1} Pb(NO$_3$)$_2$, recorded at 20 mV s^{-1} and at 20 °C.

The lead stripping from other gold surfaces with high-index facets (Figure 8) is investigated by Hamelin et al. [27]. The evolution of the curves through a zone of stereographic triangle (in Figure 8) is shown. Each stepped surface is also described as TLK (terrace, ledge, kink) notation. In Figure 8a

(zone (1 1 1)-(1 1 0)), the characteristic peak of lead stripping from (1 1 1) terraces decreases gradually, while a broader peak increases due to the stripping from the steps. An inversion of the nature of the step and terrace takes place at (3 3 1) facets. It should be taken into account that (1 1 0) is a stepped surface, as is 2(1 1 1)-(1 1 1). In Figure 8b (zone (1 1 0)-(1 0 0)), the stripping peak of lead from (1 0 0) terraces decreases progressively, as the facets are closer to (1 1 0). The (2 1 0) facet appears as a turning point of the zone (1 1 0)-(1 0 0). In Figure 8c (zone (1 0 0)-(1 1 1)), the evolution of the stripping curves are the same as the previous one, again with a turning point for the (3 1 1) facet.
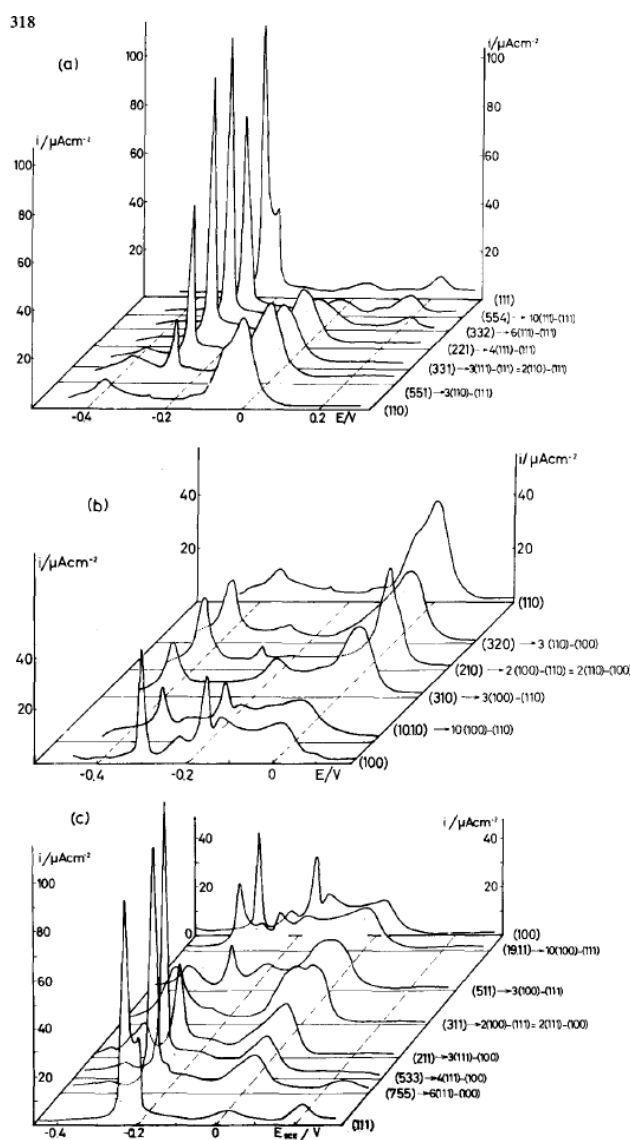

Figure 8. Cyclic voltammograms for the stripping of Pb_{upd} on Au(h k l) electrodes in 10 mmol L^{-1} $HClO_4$ + 1 mmol L^{-1} PbF_2. Au(h k l) surfaces are from the three main zones of the projected stereographic triangle: (**a**) (1 1 1)-(1 1 0) zone, (**b**) (1 1 0)-(1 0 0) zone, and (**c**) (1 0 0)-(1 1 1) zone. All the surfaces are identified with Miller index notation and with the step notation. Reprinted from reference [27]. Copyright (1984) with permission from Elsevier.

Pb_{upd} on single-crystals has also been investigated in alkaline media for surface characterization applications. It was observed that the pH affects the position of the deposition/stripping peaks because of the different chemical states of lead: Pb^{2+} in acid media and $Pb(OH)_3^-$ in alkaline media. The charge values associated with the deposition of a monolayer of lead in 0.1 mol L^{-1} NaOH +

1 mmol L^{-1} Pb(NO$_3$)$_2$ media are 444 µC cm^{-2} for (1 1 1), 340 µC cm^{-2} for (1 0 0) and 330 µC cm^{-2} for (1 1 0) [75], respectively.

Figure 9 shows the cyclic voltammograms of three low-index Au single-crystals in alkaline media [75]. Different behaviors were observed for each orientation. On Au(1 1 1), a single sharp deposition peak (0.380 V vs. RHE) was observed, while its associated stripping peak occurs at 0.435 V vs. RHE. In the case of Au(1 0 0) electrode, two peaks were associated with the Pb$_{upd}$. The main peak occurs at 0.430 V vs. RHE and the smaller one at 0.380 V vs. RHE. The two peaks associated with the dissolution of lead are recorded at 0.385 and 0.475 V vs. RHE. For the Au(1 1 0) electrode, the peaks associated with the deposition and stripping of lead are much broader and less defined than those of the previous orientations. The process is more sluggish on an Au(1 1 0) surface.
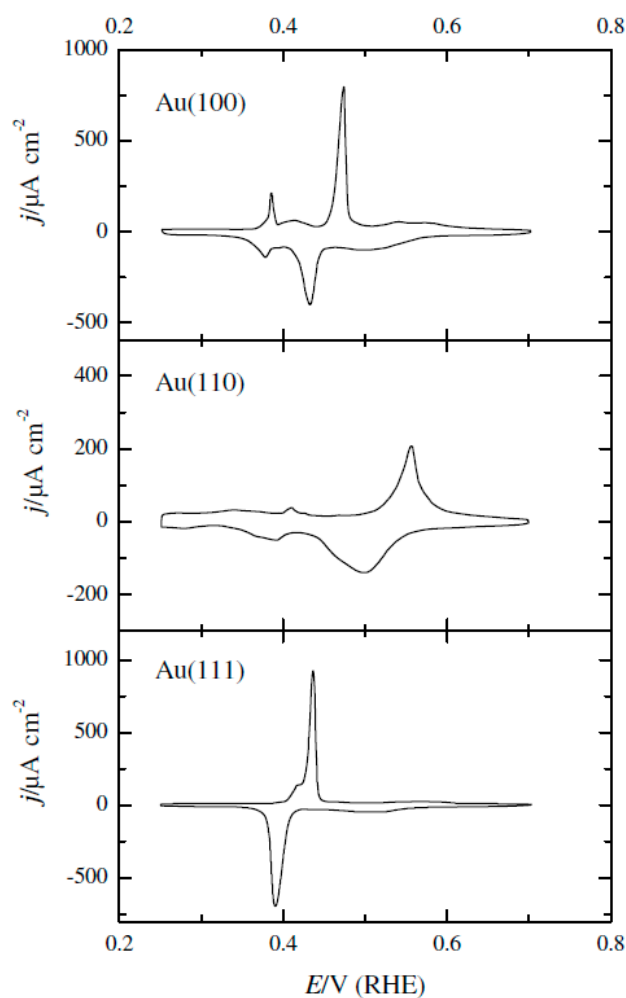

Figure 9. Cyclic voltammograms of Au(1 0 0), Au(1 1 0), and Au(1 1 1) in 0.1 mol L^{-1} NaOH + 1 mmol L^{-1} Pb(NO$_3$)$_2$ at 50 mV s^{-1}. Reprinted from reference [75]. Copyright (2004) with permission from Elsevier.

Pb$_{upd}$ has been reported to characterize bimetallic surface like for Au-Ag, as the Pb$_{upd}$ is also favorable on silver surfaces [35,76]. This technique can be used to quantify the surface coverage of gold and silver in an Au-Ag catalyst, based on the dependence of the deposited lead charge density on the nature of the underlying substrate. Indeed, the coverage of silver on the gold electrode affects the Pb$_{upd}$. Two peaks are observed during the stripping of adsorbed lead (Figure 10), the first one at −0.02 V vs. SHE, which is clearly influenced by the silver coverage (θ_{Ag}). The calculations of the charge densities corresponding to the Pb$_{upd}$ can be made from the cyclic voltammograms. A charge density

of 290 µC cm^{-2} was obtained for a bare gold electrode, while a value of 385 µC cm^{-2} was calculated on Ag$_{upd}$-modified gold. The difference of charge densities for the two surfaces may be due to the difference in the availability of sites of lead deposition or to the different adsorption energies [4]. The coverage of silver can be estimated with the following equation:

$$\theta_{Ag}Q_{Pb\text{-}Ag} + \theta_{Au}Q_{Pb\text{-}Au} = Q_{net},\qquad(3)$$

where $Q_{Pb\text{-}Ag}$ represents the charge density of Pb$_{upd}$ on silver (385 µC cm^{-2}), $Q_{Pb\text{-}Au}$ is the charge density of lead *upd* on gold (290 µC cm^{-2}), Q_{net} is the total charge density (subtracted with background current), and θ_{Au} and θ_{Ag} are the gold and silver surface coverages, respectively (with $\theta_{Au} + \theta_{Ag} = 1$).
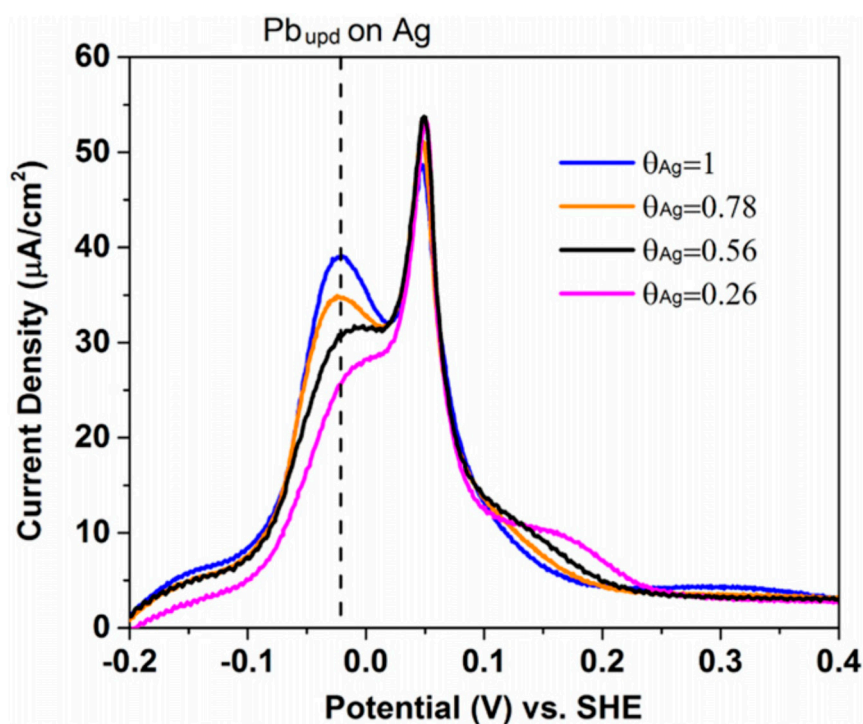

Figure 10. Lead stripping voltammetric curves of Ag$_{upd}$-modified Au with different coverages (θ_{Ag}) in 10 mmol L^{-1} HClO$_4$ + 0.2 mmol L^{-1} Pb(ClO$_4$)$_2$ at 20 mV s^{-1}. Reprinted from reference [76]. Copyright (2017) with permission from Elsevier.

3.1.3. Probing Gold Nanoparticles Surface by upd

Pb$_{upd}$ appears to be an efficient tool to characterize the surface of gold nanoparticles (AuNPs). However, contrary to single-crystal surfaces, AuNPs exhibit generally different planes on their surface. Moreover, synthesis of nanoparticles requires the use of shape-directing agents as surfactants. Pb$_{upd}$ in alkaline media can be employed to verify the cleanliness of NPs' surface and oxidize adsorbed organics on their surface [75]. The surfactant species are oxidized at potential higher than 1.20 V vs. RHE. The advantage of working in alkaline media is that PbO$_2$ deposition takes place at potentials lower than 1.10 V vs. RHE, which is lower than the onset potential for the formation of gold oxides. Gold surface is protected by these species, avoiding its oxidation which can modify its surface, while organic species are oxidized.

The Pb$_{upd}$ has been performed on AuNPs with different shapes and crystallographic orientations [74,77–79]. Hebie et al. [74] have clearly shown the shape dependence of Pb deposition/stripping on AuNPs. Indeed, Figure 11 shows cyclic voltammograms of Pb$_{upd}$ on different AuNPs—nanorods (AuNRs), nanocubes (AuNCs), and nanospheres (AuNSs). The peak associated with the lead stripping from (1 0 0) facets is clearly seen for AuNCs. It is well known that cubic NPs

are enclosed by (1 0 0) facets [80]. As the AuNCs studied in this case possess truncated edges, lead stripping is also observed for (1 1 1) and (1 1 0) planes.
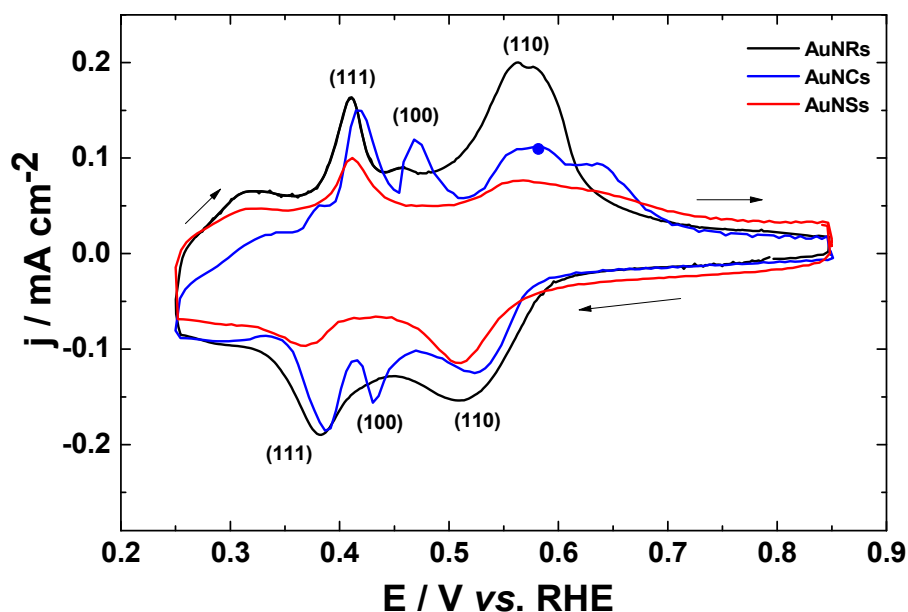
Figure 11. Cyclic voltammograms of different AuNPs (nanospheres AuNSs, nanorods AuNRs, and nanocubes AuNCs) in 0.1 mol L^{-1} NaOH + 1 mmol L^{-1} Pb(NO$_3$)$_2$ recorded at 20 mV s^{-1} and at 20 °C.

A recent study dealt with the Pb$_{upd}$ on quasi-spherical and faceted AuNPs [81]. These investigations have revealed a typical split stripping peak associated with Au(1 1 1) facets in the case of faceted AuNPs, and a single peak in the case of spherical ones. The split peak results from a sluggish kinetics of lead dissolution [82]. It appears that in the case of small terraces with more steps and defects, this doublet stripping peak is not observed, contrary to the peak obtained with faceted NPs. The study suggests that introducing a degree of roughness on (1 1 1) terraces by potential cycles can suppress the splitting profile. The splitting of the peak associated with the desorption from (1 1 1) terraces can be used as an indication of the surface crystallinity of polyfaceted AuNPs.

Thallium is also used for *upd* process on gold nanoparticles. It is known to be used for characterizing AuNPs with defined shapes (nanocrystals) [83,84]. Tl$_{upd}$ has been employed to check the surface cleanliness and the crystallinity of these nanocrystals before performing an oxygen reduction reaction.

3.2. Case of Pt

3.2.1. H$_{upd}$ on Pt

The famous *upd* process widely studied on platinum is the *upd* of hydrogen (H$_{upd}$) [85,86]. H$_{upd}$ is not strictly an *upd* process but the adsorption of hydrogen on the surface. The H$_{upd}$ region acts as a fingerprint for platinum surfaces. Indeed, the profile of the hydrogen adsorption/desorption region obtained by cyclic voltammogram permits an indication of the facets, to assess the active surface area and also to ensure the cleanliness of electrode and cell. Combined with the adsorption of organic molecule, it permits determining the surface coverage. The underpotential deposition of metals can give complementary information to quantify the crystallographic orientations [47]. Traditionally, the Electrochemical Active Surface Area (ECSA) of platinum is determined by the charge corresponding to the H$_{upd}$. Indeed, one platinum atom has the ability to adsorb one hydrogen atom. The charge associated with H$_{upd}$ indicates the number of platinum atoms at the surface. The density of charge associated with the formation of a monolayer of hydrogen depends on the crystallographic orientations,

and the value of 210 µC cm^{-2} is the average value for polycrystalline platinum [87,88]. CO-stripping is also used as a method to calculate the ECSA of platinum in acid media [89]. It is important to notice that in acid media, the number of electrons per site during the adsorption of CO on platinum is equal to 2.

The development of bimetallic surfaces for catalysis requests to determine ECSA values. In the case of ruthenium-containing catalysts, H$_{upd}$ is not suitable because of the overlap of the hydrogen and ruthenium oxidation currents [90]. Moreover, hydrogen can be absorbed in the Ru oxide lattice, leading to more than one monolayer of hydrogen. CO-stripping on bimetallic Pt-Ru surface appears to be suitable, however, the adsorption modes on both platinum and ruthenium needs to be deeply elucidated. The mode of adsorption is an important parameter to calculate the charge.

3.2.2. Bi on Pt: A Probe for (1 1 1) Planes

It has been shown that bismuth is spontaneously adsorbed on a platinum surface when the electrode is simply put in contact with a solution containing a salt of Bi(III) species [44]. When a linear potential sweep is applied to the electrode, the oxidized and reduced forms of this compound stay adsorbed at the platinum surface. For the planes (1 1 1), (1 0 0), and (1 1 0), the oxidation peaks are located at 0.610 V vs. RHE, 0.825 V vs. RHE, and 0.915 V vs. RHE, respectively. Bi$_{upd}$ appears as a tool to highlight the presence of (1 1 1) facets, especially when the surface exhibits a combination of several planes. It has been proposed that one atom of bismuth covers three atoms of platinum [47]:

$$Pt_3(1\ 1\ 1)\text{-Bi} + 2H_2O = Pt_3(1\ 1\ 1)\text{-Bi(OH)}_2 + 2H^+ + 2e^-. \tag{4}$$
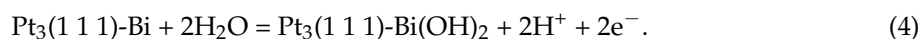
In the case of stepped surfaces, the redox peak associated with the adsorption of bismuth on (1 1 1) terraces sites gives a charge which is proportional to the number of (1 1 1) terrace sites, without interference from adsorbed bismuth to another site [47]. The adsorption of bismuth suppresses the H$_{upd}$ region, which means that H adsorption sites on platinum are fully blocked.

To characterize the (1 1 1) sites belonging to terrace domains, the charge density values of each surface are obtained by integrating the voltammetric peaks. Figure 12 shows the plots of the charge underneath the bismuth redox peak (q_{Bi}) *versus* the calculated terrace charge [47]. The calculation of the terrace charge depends on how bismuth is adsorbed on the step and terrace sites. Bismuth is preferentially adsorbed on step sites, so the adsorption takes place on the terraces when all the step sites have been covered [91]. A linear equation is obtained and can be used to calibrate the (1 1 1) terrace sites:

$$q_{Bi} = (0.64 \pm 0.02)q_t(1\ 1\ 1) \tag{5}$$
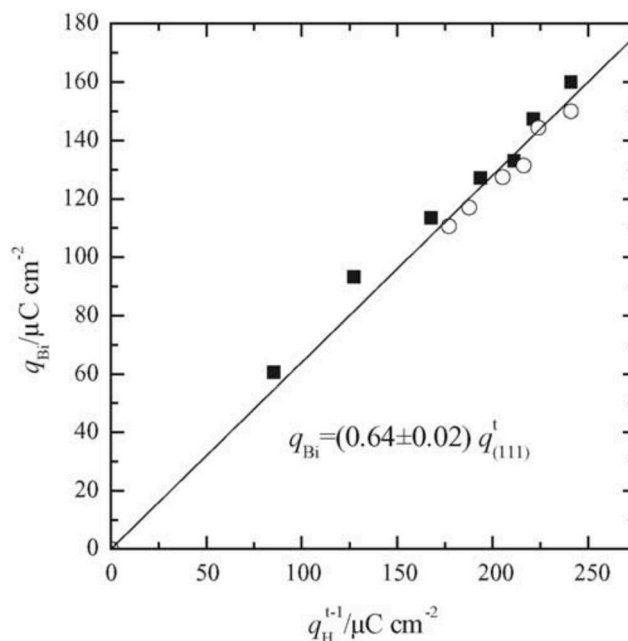
Figure 12. Charge density values of the bismuth redox peak vs. the charge associated with the (1 1 1) sites on the terraces, assuming that one electron is exchanged per site (■: Pt(n,n,n−2), ○: Pt(n+1,n−1,n−1) electrodes). Reprinted from reference [47]. Copyright (2005) with permission from Elsevier.

3.2.3. Ge on Pt: A Probe for (1 0 0) Planes

The *spontaneous deposition* of germanium (Ge_{upd}) acts as a complementary tool to Bi_{upd} to characterize platinum surfaces. It has been proposed that one atom of germanium covers four atoms of platinum and the equation of the oxidation of adsorbed germanium on platinum can be written as follows:

$$Pt_4(1\,0\,0)\text{-}Ge + H_2O = Pt_4(1\,0\,0)\text{-}GeO + 2H^+ + 2e^-. \tag{6}$$
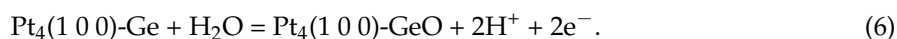
As for Bi_{upd}, the oxidation of a spontaneously deposited layer of germanium on a platinum surface will give information about the crystallographic orientations of the surface [46]. The H_{upd} is completely inhibited when a full layer of germanium is deposited (Figure 13). Conversely, the H_{upd} is partially inhibited when the surface is not fully covered by germanium. The sharp reversible peaks at 0.540 V vs. RHE are associated with germanium ad-atoms on the (1 0 0) plane. During continuous cycling between 0.060 and 0.600 V vs. RHE, the voltammetric profile remains stable, meaning that the germanium species are still adsorbed on the surface. Moreover, the pH value of the electrolyte does not affect the peaks, suggesting that a germanium oxide is formed.
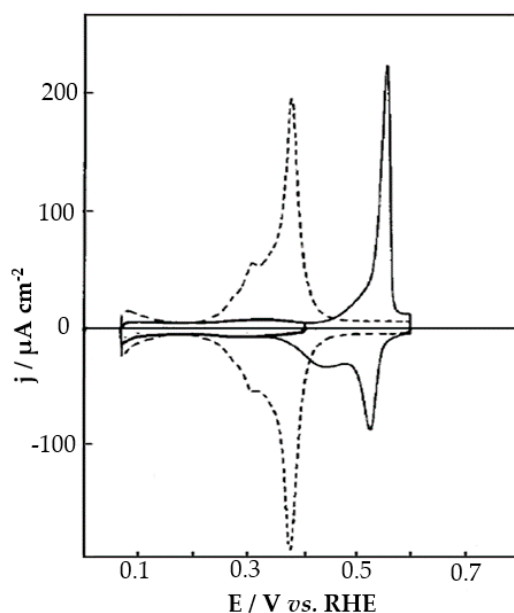
Figure 13. Voltammograms of a Pt(1 0 0) surface fully covered with Ge (continuous line) and Pt(1 0 0) blank. Reprinted from Reference [46]. Copyright (1992) with permission from Elsevier.

The (1 1 0) plane does not show a reversible oxidation/reduction process but a quick desorption is observed. For (1 1 1) planes, the oxidation peak is centered at 0.730 V vs. RHE. However, the oxidation makes a partial dissolution of the germanium layer.

Germanium appears to be sensitive to (1 0 0) planes. Conversely to bismuth, germanium is not irreversibly adsorbed on Pt and it is possible to recover the hydrogen region following the experiment.

As for the study related to (1 1 1) terraces toward bismuth adsorption, adsorbed germanium can be used to characterize (1 0 0) terraces sites of stepped platinum surfaces [47,48].

A linear equation can also be obtained to calibrate terrace sites, as for bismuth on (1 1 1) terraces:

$$q_{Ge} = (0.56 \pm 0.03)qt(1\ 0\ 0). \tag{7}$$

3.2.4. Cu on Pt: A Tool to Characterize Bimetallic Surfaces

As it was reported in this mini review, Cu_{upd} is so far, one of the most studied systems on low-index single-crystals as well as on stepped surfaces [92]. As for gold surfaces, Cu_{upd} on platinum is strongly dependent of the anions present in the electrolyte [17,93]. However, there are only few investigations about its application as a tool for surface characterization. Cu_{upd} is a suitable technique to calculate electrochemical active surface area (ECSA) of Pt and alloys containing Pt. Indeed, Cu_{upd} has been proposed to characterize the bimetallic Pt-Ru surfaces. The integration of the copper stripping peak area permits the estimation of ECSA. It has been shown that Cu_{upd} is an accurate tool to estimate ECSA of each platinum and ruthenium in Pt–Ru electrodes. The coverage of ruthenium can also be determined by this method. Cu_{upd} has also been reported for the calculation of ECSA of Pt-Pd alloys [94]. Indeed, copper is a suitable ad-atom to deposit because its adsorption occurs at a potential region where no other Faradaic reaction takes place on both platinum and palladium.

3.2.5. Probing the Surface of Pt Nanoparticles

Bi_{upd} and Ge_{upd} were also investigated on platinum nanoparticles to probe their surface [47,95–97]. In the case of nanoparticles containing (1 1 1) and (1 0 0) planes, the fraction of each domain is obtained by the ratio of the Faradaic charge of germanium ($Q_{f,Ge}$) or bismuth ($Q_{f,Bi}$) with the charge associated with the hydrogen desorption process ($Q_{f,H}$). The characterization of PtNPs prepared in different

conditions has been reported [98]. The use of Ge_{upd} and Bi_{upd} permitted determining the percentage of (1 0 0) and (1 1 1) facets, respectively. The fraction of (1 1 0) sites has been estimated. Indeed, the peak of H_{upd} associated with (1 1 0) facets decreases, while the difference from 100% of the sum of (1 1 1) and (1 0 0) facets decreases.

3.3. Case of Pd

Cu on Pd

There are only a few studies about *upd* of metals on palladium surfaces [11,40]. This is due to the difficulty for metal monolayers to be adsorbed on the double-layer region, which is narrow [99]. Palladium also has the ability to absorb hydrogen in its bulk, this process may mask the *upd* one. It should be noted that there is no study about *upd* of metals to characterize palladium surfaces. For example, Cu grows epitaxially with the Pd substrate.

Cu_{upd} has been studied on polycrystalline and single-crystalline palladium electrodes [100]. This study has shown that, under adequate conditions, Cu adsorption can be restricted to a potential range where no other Faradaic reaction takes place. Cu_{upd} on palladium surfaces occurs at potentials lower than the onset potential of oxides formation, and hydrogen absorption is inhibited by changing the pH of the electrolyte. Figure 14 shows the cyclic voltammograms of *upd*/stripping on palladium (1 0 0) and (1 1 1) single-crystal and polycrystalline palladium. It is clearly seen that the single-crystal electrode present less complex voltammograms than polycrystalline palladium. On Pd(1 1 1), the *upd* and desorption processes give a single sharp peak (A_3/D_3) preceded by a small shoulder. On Pd(1 0 0), two peaks are observed (A_2/D_2 and A_6/D_6) and a small shoulder noted A_1/D_1. The complexity of the voltammogram obtained on polycrystalline palladium is due to the variety of crystal planes.
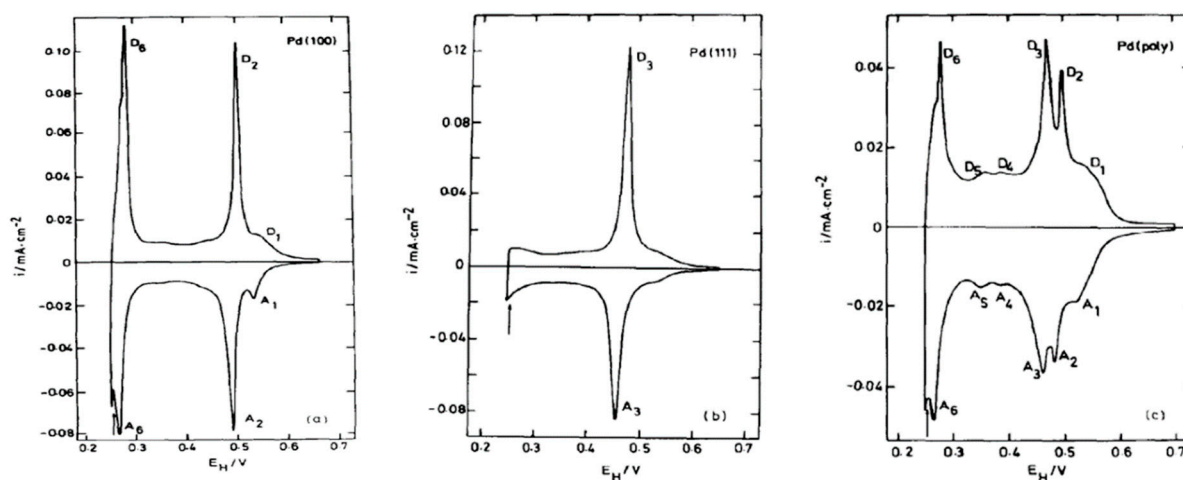
Figure 14. Cyclic voltammograms of Pd single-crystal electrodes in 0.5 mol L^{-1} $NaClO_4$ + 0.01 mol L^{-1} $HClO_4$ + 1 mmol L^{-1} Cu^{2+}, at 10 mV s^{-1}: (**a**) Pd(1 0 0), (**b**) Pd(1 1 1), and (**c**) polycrystalline Pd. Reprinted from reference [100]. Copyright (1988) with permission from Elsevier.

4. Conclusions

Investigations on *upd* of transition metals at noble metal surfaces have been increasing over these last two decades. It appears to be a powerful electrochemical tool to probe and characterize the working electrode surface. Indeed, *upd* techniques have been reported to calculate electrochemical active surface area, especially in the case of bimetallic surface, and to probe the crystallographic orientations among the surface of single-crystals and nanoparticles. Pb_{upd} is mostly used to characterize the orientation of gold nanoparticles and surfaces. In the case of platinum surfaces, the probe of crystallographic

orientation is made with bismuth and germanium adsorption. Cu_{upd} is one of the most studied *upd* systems that appear to be useful for characterizing the surface of bimetallic materials.

References

1. Scortichnini, C.L.; Reilley, C.N. Surface characterization of Pt electrodes using underpotential deposition of H and Cu: Part I. Pt(100). *J. Electroanal. Chem.* **1982**, *139*, 233–245. [CrossRef]
2. Bockris, J.M.; Nagy, Z.; Damjanovic, A. On the deposition and dissolution of zinc in alkaline solutions. *J. Electrochem. Soc.* **1972**, *119*, 285–295. [CrossRef]
3. Kolb, D.; Przasnyski, M.; Gerischer, H. Underpotential deposition of metals and work function differences. *J. Electroanal. Chem.* **1974**, *54*, 25–38. [CrossRef]
4. Kirowa-Eisner, E.; Bonfil, Y.; Tzur, D.; Gileadi, E. Thermodynamics and kinetics of UPD of lead on polycrystalline silver and gold. *J. Electroanal. Chem.* **2003**, *552*, 171–183. [CrossRef]
5. Szabó, S. Underpotential deposition of metals on foreign metal substrates. *Int. Rev. Phys. Chem.* **1991**, *10*, 207–248. [CrossRef]
6. Swathirajan, S.; Bruckenstein, S. Thermodynamics and kinetics of underpotential deposition of metal monolayers on polycrystalline substrates. *Electrochim. Acta* **1983**, *28*, 865–877. [CrossRef]
7. Leiva, E. Recent developments in the theory of metal upd. *Electrochim. Acta* **1996**, *41*, 2185–2206. [CrossRef]
8. Rojas, M.I.; Dassie, S.A.; Leiva, E.P.M. Theoretical-study about the adsorption of lead on (111), (100), (110) monocrystalline surfaces of gold. *Z. Phys. Chem.* **1994**, *185*, 33–50. [CrossRef]
9. Kolb, D.M.; Schneider, J. Surface reconstruction in electrochemistry: Au(100-(5 × 20), Au(111)-(1 × 23) and Au(110)-(1 × 2). *Electrochim. Acta* **1986**, *31*, 929–936. [CrossRef]
10. Oviedo, O.A.; Reinaudi, L.; García, S.G.; Leiva, E.P.M. Experimental techniques and structure of the underpotential deposition phase. In *Underpotential Deposition*; Scholz, F., Ed.; Springer: Cham, Switzerland, 2016; pp. 17–89.
11. Szabó, S.; Bakos, I.; Nagy, F.; Mallát, T. Study of the underpotential deposition of copper onto polycrystalline palladium surfaces. *J. Electroanal. Chem.* **1989**, *263*, 137–146. [CrossRef]
12. Engelsmann, K.; Lorenz, W.J.; Schmidt, E. Underpotential deposition of lead on polycrystalline and single-crystal gold surfaces: Part I. Thermodynamics. *J. Electroanal. Chem.* **1980**, *114*, 1–10. [CrossRef]
13. Garcia, S.; Salinas, D.; Mayer, C.; Schmidt, E.; Staikov, G.; Lorenz, W.J. Ag UPD on Au(100) and Au(111). *Electrochim. Acta* **1998**, *43*, 3007–3019. [CrossRef]
14. Rooryck, V.; Reniers, F.; Buess-Herman, C.; Attard, G.A.; Yang, X. The silver UPD on gold(111) revisited. *J. Electroanal. Chem.* **2000**, *482*, 93–101. [CrossRef]
15. Hachiya, T.; Honbo, H.; Itaya, K. Detailed underpotential deposition of copper on gold(111) in aqueous-solutions. *J. Electroanal. Chem.* **1991**, *315*, 275–291. [CrossRef]
16. Uchida, H.; Hiei, M.; Watanabe, M. Electrochemical quartz crystal microbalance study of copper adatoms on Au(111) electrodes in solutions of perchloric and sulfuric acid. *J. Electroanal. Chem.* **1998**, *452*, 97–106. [CrossRef]
17. Herrero, E.; Glazier, S.; Buller, L.J.; Abruña, H.D. X-ray and electrochemical studies of Cu upd on single crystal electrodes in the presence of bromide: Comparison between Au(111) and Pt(111) electrodes. *J. Electroanal. Chem.* **1999**, *461*, 121–130. [CrossRef]
18. Nakamura, M.; Endo, O.; Ohta, T.; Ito, M.; Yoda, Y. Surface X-ray diffraction study of Cu UPD on Au (1 1 1) electrode in 0.5 M H_2SO_4 solution: The coadsorption structure of UPD copper, hydration water molecule and bisulfate anion on Au (1 1 1). *Surf. Sci.* **2002**, *514*, 227–233. [CrossRef]
19. Kuzume, A.; Herrero, E.; Feliu, J.M.; Nichols, R.J.; Schiffrin, D.J. Copper underpotential deposition at high index single crystal surfaces of Au. *J. Electroanal. Chem.* **2004**, *570*, 157–161. [CrossRef]
20. Danilov, A.I.; Molodkina, E.B.; Rudnev, A.V.; Polukarov, Y.M.; Feliu, J.M. Kinetics of copper deposition on Pt(111) and Au(111) electrodes in solutions of different acidities. *Electrochim. Acta* **2005**, *50*, 5032–5043. [CrossRef]

21. Madry, B.; Wandelt, K.; Nowicki, M. Deposition of copper and sulfate on Au(111): New insights. *Appl. Surf. Sci.* **2016**, *388*, 678–683. [CrossRef]
22. Madry, B.; Wandelt, K.; Nowicki, M. Sulfate structures on copper deposits on Au(111): In situ STM investigations. *Electrochim. Acta* **2016**, *217*, 249–261. [CrossRef]
23. Sebastián, P.; Gómez, E.; Climent, V.; Feliu, J.M. Copper underpotential deposition at gold surfaces in contact with a deep eutectic solvent: New insights. *Electrochem. Commun.* **2017**, *78*, 51–55. [CrossRef]
24. Yang, M.Z.; Zhang, H.X.; Deng, Q.B. Understanding the copper underpotential deposition process at strained gold surface. *Electrochem. Commun.* **2017**, *82*, 125–128. [CrossRef]
25. Dursun, Z.; Ben Aoun, S.; Taniguchi, I. Electrocatalytic oxidation of D-glucose using a Cd ad-atom-modified Au(111) electrode in alkaline solution. *Turk. J. Chem.* **2008**, *32*, 423–430.
26. Adžić, R.; Yeager, E.; Cahan, B.D. Optical and electrochemical studies of underpotential deposition of lead on gold evaporated and single-crystal electrodes. *J. Electrochem. Soc.* **1974**, *121*, 474–484. [CrossRef]
27. Hamelin, A.; Lipkowski, J. Underpotential deposition of lead on gold single-crystal faces: Part 2. General discussion. *J. Electroanal. Chem.* **1984**, *171*, 317–330. [CrossRef]
28. Hamelin, A. Underpotential deposition of lead on single-crystal faces of gold: Part 1. The influence of crystallographic orientation of the substrate. *J. Electroanal. Chem.* **1984**, *165*, 167–180. [CrossRef]
29. Samant, M.G.; Toney, M.F.; Borges, G.L.; Blum, L.; Melroy, O.R. Grazing incidence x-ray diffraction of lead monolayers at a silver (111) and gold (111) electrode/electrolyte interface. *J. Phys. Chem.* **1988**, *92*, 220–225. [CrossRef]
30. Feliu, J.; Fernandez-Vega, A.; Orts, J.; Aldaz, A. The behaviour of lead and bismuth adatoms on well-defined platinum surfaces. *J. Chim. Phys.* **1991**, *88*, 1493–1518. [CrossRef]
31. Wang, J.X.; Adzic, R.R.; Ocko, B.M. X-ray scattering study of Tl adlayers on the Au(111) electrode in alkaline solutions: Metal monolayer, OH⁻ coadsorption, and oxide formation. *J. Phys. Chem.* **1994**, *98*, 7182–7190. [CrossRef]
32. Wheeler, D.R.; Wang, J.X.; Adžić, R.R. The effects of anions on the underpotential deposition of Tl on Pt(111): A voltammetric study. *J. Electroanal. Chem.* **1995**, *387*, 115–119. [CrossRef]
33. Batchelor-McAuley, C.; Wildgoose, G.G.; Compton, R.G. The contrasting behaviour of polycrystalline bulk gold and gold nanoparticle modified electrodes towards the underpotential deposition of thallium. *New J. Chem.* **2008**, *32*, 941–946. [CrossRef]
34. Rodriguez, P.; García-Aráez, N.; Herrero, E.; Feliu, J.M. New insight on the behavior of the irreversible adsorption and underpotential deposition of thallium on platinum (111) and vicinal surfaces in acid electrolytes. *Electrochim. Acta* **2015**, *151*, 319–325. [CrossRef]
35. Bonfil, Y.; Brand, M.; Kirowa-Eisner, E. Characteristics of subtractive anodic stripping voltammetry of lead, cadmium and thallium at silver-gold alloy electrodes. *Electroanalysis* **2003**, *15*, 1369–1376. [CrossRef]
36. Brust, M.; Ramirez, S.A.; Gordillo, G.J. Site-specific modification of gold nanoparticles by underpotential deposition of cadmium atoms. *ChemElectroChem* **2018**, *5*, 1586–1590. [CrossRef]
37. Abaci, S.; Zhang, L.; Shannon, C. The influence of counter anions on the underpotential deposition of mercury(II) on Au(111): Temperature-dependent studies. *J. Electroanal. Chem.* **2004**, *571*, 169–176. [CrossRef]
38. Rodes, A.; Herrero, E.; Feliu, J.M.; Aldaz, A. Structure sensitivity of irreversibly adsorbed tin on gold single-crystal electrodes in acid media. *J. Chem. Soc. Faraday Trans.* **1996**, *92*, 3769–3776. [CrossRef]
39. Meier, L.A.; Salinas, D.R.; Feliu, J.M.; García, S.G. Spontaneous deposition of Sn on Au(1 1 1). An in situ STM study. *Electrochem. Commun.* **2008**, *10*, 1583–1586. [CrossRef]
40. Szabo, S. Investigations of copper, silver and bismuth deposition on palladium in perchloric acid media. *J. Electroanal. Chem.* **1977**, *77*, 193–203. [CrossRef]
41. Adžić, R.; Jovančićević, V.; Podlavicky, M. Optical and electrochemical study of underpotential deposition of bismuth on gold electrode. *Electrochim. Acta* **1980**, *25*, 1143–1146. [CrossRef]
42. Ganon, J.P.; Clavilier, J. Electrical resistance measurement in electrochemical adsorption experiments of lead and bismuth on thin films of gold. II. *Surf. Sci.* **1984**, *147*, 583–598. [CrossRef]
43. Ganon, J.P.; Clavilier, J. Electrochemical adsorption of lead and bismuth at gold single crystal surfaces with vicinal (111) orientations. I. *Surf. Sci.* **1984**, *145*, 487–518. [CrossRef]
44. Clavilier, J.; Feliu, J.; Aldaz, A. An irreversible structure sensitive adsorption step in bismuth underpotential deposition at platinum electrodes. *J. Electroanal. Chem.* **1988**, *243*, 419–433. [CrossRef]

45. Thiel, K.-O.; Hintze, M.; Vollmer, A.; Donner, C. Bismuth UPD on the modified Au (1 1 1) electrode. *J. Electroanal. Chem.* **2010**, *638*, 143–150. [CrossRef]

46. Gómez, R.; Llorca, M.; Feliu, J.; Aldaz, A. The behaviour of germanium adatoms irreversibly adsorbed on platinum single crystals. *J. Electroanal. Chem.* **1992**, *340*, 349–355. [CrossRef]

47. Rodriguez, P.; Herrero, E.; Solla-Gullon, J.; Vidal-Iglesias, F.J.; Aldaz, A.; Feliu, J.M. Specific surface reactions for identification of platinum surface domains - Surface characterization and electrocatalytic tests. *Electrochim. Acta* **2005**, *50*, 4308–4317. [CrossRef]

48. Rodríguez, P.; Herrero, E.; Solla-Gullón, J.; Vidal-Iglesias, F.; Aldaz, A.; Feliu, J. Electrochemical characterization of irreversibly adsorbed germanium on platinum stepped surfaces vicinal to Pt (1 0 0). *Electrochim. Acta* **2005**, *50*, 3111–3121. [CrossRef]

49. Gooyoung, J.; Choong Kyun, R. Two electrochemical processes for the deposition of Sb on Au(100) and Au(111): Irreversible adsorption and underpotential deposition. *J. Electroanal. Chem.* **1997**, *436*, 277–280. [CrossRef]

50. Chen, Y.; Wang, L.S.; Pradel, A.; Ribes, M.; Record, M.C. A voltammetric study of the underpotential deposition of cobalt and antimony on gold. *J. Electroanal. Chem.* **2014**, *724*, 55–61. [CrossRef]

51. Chen, Y.; Wang, L.S.; Pradel, A.; Merlen, A.; Ribes, M.; Record, M.C. Underpotential deposition of selenium and antimony on gold. *J. Solid State Electrochem.* **2015**, *19*, 2399–2411. [CrossRef]

52. Vaskevich, A.; Sinapi, F.; Mekhalif, Z.; Delhalle, J.; Rubinstein, I. Underpotential deposition of nickel on {111}-textured gold electrodes in dimethyl sulfoxide. *J. Electrochem. Soc.* **2005**, *152*, C744–C750. [CrossRef]

53. Hebie, S.; Napporn, T.W.; Kokoh, K.B. Beneficial promotion of underpotentially deposited lead adatoms on gold nanorods toward glucose electrooxidation. *Electrocatalysis* **2017**, *8*, 67–73. [CrossRef]

54. Alvarez-Rizatti, M.; Jüttner, K. Electrocatalysis of oxygen reduction by UPD of lead on gold single-crystal surfaces. *J. Electroanal. Chem.* **1983**, *144*, 351–363. [CrossRef]

55. Parpot, P.; Kokoh, K.B.; Beden, B.; Belgsir, E.M.; Leger, J.M.; Lamy, C. Selective electrocatalytic oxidation of sucrose on smooth and upd-lead modified platinum-electrodes in alkaline-medium. *Stud. Surf. Sci. Catal.* **1993**, *78*, 439–445.

56. Kokoh, K.; Léger, J.-M.; Beden, B.; Lamy, C. "On line" chromatographic analysis of the products resulting from the electrocatalytic oxidation of d-glucose on Pt, Au and adatoms modified Pt electrodes—Part I. Acid and neutral media. *Electrochim. Acta* **1992**, *37*, 1333–1342. [CrossRef]

57. Chen, H.M.; Xing, Z.L.; Zhu, S.Q.; Zhang, L.L.; Chang, Q.W.; Huang, J.L.; Cai, W.B.; Kang, N.; Zhong, C.J.; Shao, M.H. Palladium modified gold nanoparticles as electrocatalysts for ethanol electrooxidation. *J. Power Sources* **2016**, *321*, 264–269. [CrossRef]

58. Vélez, P.; Cuesta, A.; Leiva, E.P.M.; Macagno, V.A. The underpotential deposition that should not be: Cu(1 × 1) on Au(111). *Electrochem. Commun.* **2012**, *25*, 54–57. [CrossRef]

59. Möller, F.; Magnussen, O.M.; Behm, R.J. CuCl adlayer formation and Cl induced surface alloying: An in situ STM study on Cu underpotential deposition on Au(110) electrode surfaces. *Electrochim. Acta* **1995**, *40*, 1259–1265. [CrossRef]

60. Holzle, M.H.; Zwing, V.; Kolb, D.M. The influence of steps on the deposition of Cu onto Au(111). *Electrochim. Acta* **1995**, *40*, 1237–1247. [CrossRef]

61. Hasegawa, Y.; Avouris, P. Manipulation of the reconstruction of the Au(111) surface with the STM. *Science* **1992**, *258*, 1763–1765. [CrossRef] [PubMed]

62. Nichols, R.J.; Kolb, D.M.; Behm, R.J. STM observations of the initial stages of copper deposition on gold single-crystal electrodes. *J. Electroanal. Chem.* **1991**, *313*, 109–119. [CrossRef]

63. Magnussen, O.M.; Hotlos, J.; Nichols, R.J.; Kolb, D.M.; Behm, R.J. Atomic structure of Cu adlayers on Au(100) and Au(111) electrodes observed by in situ scanning tunneling microscopy. *Phys. Rev. Lett.* **1990**, *64*, 2929–2932. [CrossRef]

64. Kongstein, O.E.; Bertocci, U.; Stafford, G.R. In situ stress measurements during copper electrodeposition on (111)-textured Au. *J. Electrochem. Soc.* **2005**, *152*, C116–C123. [CrossRef]

65. Hagenström, H.; Schneeweiss, M.A.; Kolb, D.M. Copper underpotential deposition on ethanethiol-modified Au(111) electrodes: Kinetic effects. *Electrochim. Acta* **1999**, *45*, 1141–1145. [CrossRef]

66. Deng, Q.; Smetanin, M.; Weissmüller, J. Mechanical modulation of reaction rates in electrocatalysis. *J. Catal.* **2014**, *309*, 351–361. [CrossRef]

67. Akhade, S.A.; McCrum, I.T.; Janik, M.J. The impact of specifically adsorbed ions on the copper-catalyzed electroreduction of CO_2. *J. Electrochem. Soc.* **2016**, *163*, F477–F484. [CrossRef]

68. Mrozek, P.; Sung, Y.-E.; Han, M.; Gamboa-Aldeco, M.; Wieckowski, A.; Chen, C.-H.; Gewirth, A.A. Coadsorption of sulfate anions and silver adatoms on the Au (111) single crystal electrode. Ex situ and in situ comparison. *Electrochim. Acta* **1995**, *40*, 17–28. [CrossRef]

69. Rouya, E.; Cattarin, S.; Reed, M.L.; Kelly, R.G.; Zangari, G. Electrochemical characterization of the surface area of nanoporous gold films. *J. Electrochem. Soc.* **2012**, *159*, K97–K102. [CrossRef]

70. Hernandez, F.; Baltruschat, H. Hydrogen evolution and CuUPD at stepped gold single crystals modified with Pd. *J. Solid State Electrochem.* **2007**, *11*, 877–885. [CrossRef]

71. Hamelin, A.; Katayama, A.; Picq, G.; Vennereau, P. Surface characterization by underpotential deposition—Lead on gold surfaces. *J. Electroanal. Chem.* **1980**, *113*, 293–300. [CrossRef]

72. Hamelin, A.; Katayama, A. Lead underpotential deposition on gold single-crystal surfaces—The (100) face and its vicinal faces. *J. Electroanal. Chem.* **1981**, *117*, 221–232. [CrossRef]

73. Hamelin, A. Lead adsorption on gold single-crystal stepped surfaces. *J. Electroanal. Chem.* **1979**, *101*, 285–290. [CrossRef]

74. Hebie, S.; Cornu, L.; Napporn, T.W.; Rousseau, J.; Kokoh, B.K. Insight on the surface structure effect of free gold nanorods on glucose electrooxidation. *J. Phys. Chem. C* **2013**, *117*, 9872–9880. [CrossRef]

75. Hernandez, J.; Solla-Gullon, J.; Herrero, E. Gold nanoparticles synthesized in a water-in-oil microemulsion: Electrochemical characterization and effect of the surface structure on the oxygen reduction reaction. *J. Electroanal. Chem.* **2004**, *574*, 185–196. [CrossRef]

76. Yu, L.; Akolkar, R. Lead underpotential deposition for the surface characterization of silver ad-atom modified gold electrocatalysts for glucose oxidation. *J. Electroanal. Chem.* **2017**, *792*, 61–65. [CrossRef]

77. Hernandez, J.; Solla-Gullon, J.; Herrero, E.; Feliu, J.M.; Aldaz, A. In situ surface characterization and oxygen reduction reaction on shape-controlled gold nanoparticles. *J. Nanosci. Nanotechnol.* **2009**, *9*, 2256–2273. [CrossRef]

78. Hebie, S.; Kokoh, K.B.; Servat, K.; Napporn, T.W. Shape-dependent electrocatalytic activity of free gold nanoparticles toward glucose oxidation. *Gold Bull.* **2013**, *46*, 311–318. [CrossRef]

79. Hebie, S.; Napporn, T.W.; Morais, C.; Kokoh, K.B. Size-dependent electrocatalytic activity of free gold nanoparticles for the glucose oxidation reaction. *ChemPhysChem* **2016**, *17*, 1454–1462. [CrossRef] [PubMed]

80. Niu, W.X.; Zheng, S.L.; Wang, D.W.; Liu, X.Q.; Li, H.J.; Han, S.A.; Chen, J.; Tang, Z.Y.; Xu, G.B. Selective synthesis of single-crystalline rhombic dodecahedral, octahedral, and cubic gold nanocrystals. *J. Am. Chem. Soc.* **2009**, *131*, 697–703. [CrossRef] [PubMed]

81. Jeyabharathi, C.; Zander, M.; Scholz, F. Underpotential deposition of lead on quasi-spherical and faceted gold nanoparticles. *J. Electroanal. Chem.* **2018**, *819*, 159–162. [CrossRef]

82. Schultze, J.; Dickertmann, D. Potentiodynamic desorption spectra of metallic monolayers of Cu, Bi, Pb, Tl, and Sb adsorbed at (111), (100), and (110) planes of gold electrodes. *Surf. Sci.* **1976**, *54*, 489–505. [CrossRef]

83. Lu, F.; Zhang, Y.; Liu, S.Z.; Lu, D.Y.; Su, D.; Liu, M.Z.; Zhang, Y.G.; Liu, P.; Wang, J.X.; Adzic, R.R.; et al. Surface proton transfer promotes four-electron oxygen reduction on gold nanocrystal surfaces in alkaline solution. *J. Am. Chem. Soc.* **2017**, *139*, 7310–7317. [CrossRef]

84. Zhang, Y.; Lu, F.; Liu, S.; Lu, D.; Su, D.; Liu, M.; Zhang, Y.; Liu, P.; Wang, J.X.; Adzic, R.R. Oxygen reduction on gold nanocrystal surfaces in alkaline electrolyte: Evidence for surface proton transfer effects. *ECS Trans.* **2018**, *85*, 93–110. [CrossRef]

85. Conway, B.; Angerstein-Kozlowska, H.; Sharp, W.; Criddle, E. Ultrapurification of water for electrochemical and surface chemical work by catalytic pyrodistillation. *Anal. Chem.* **1973**, *45*, 1331–1336. [CrossRef]

86. Zolfaghari, A.; Chayer, M.; Jerkiewicz, G. Energetics of the underpotential deposition of hydrogen on platinum electrodes I. Absence of coadsorbed species. *J. Electrochem. Soc.* **1997**, *144*, 3034–3041. [CrossRef]

87. Clavilier, J.; Orts, J.M.; Gómez, R.; Feliu, J.M.; Aldaz, A. Comparison of electrosorption at activated polycrystalline and Pt(531) kinked platinum electrodes: Surface voltammetry and charge displacement on potentiostatic CO adsorption. *J. Electroanal. Chem.* **1996**, *404*, 281–289. [CrossRef]

88. Chen, Q.-S.; Solla-Gullón, J.; Sun, S.-G.; Feliu, J.M. The potential of zero total charge of Pt nanoparticles and polycrystalline electrodes with different surface structure: The role of anion adsorption in fundamental electrocatalysis. *Electrochim. Acta* **2010**, *55*, 7982–7994. [CrossRef]

89. Maillard, F.; Savinova, E.R.; Stimming, U. CO monolayer oxidation on Pt nanoparticles: Further insights into the particle size effects. *J. Electroanal. Chem.* **2007**, *599*, 221–232. [CrossRef]

90. Green, C.L.; Kucernak, A. Determination of the platinum and ruthenium surface areas in platinum−ruthenium alloy electrocatalysts by underpotential deposition of copper. I. Unsupported catalysts. *J. Phys. Chem. B* **2002**, *106*, 1036–1047. [CrossRef]

91. Herrero, E.; Climent, V.C.; Feliu, J.M. On the different adsorption behavior of bismuth, sulfur, selenium and tellurium on a Pt (775) stepped surface. *Electrochem. Commun.* **2000**, *2*, 636–640. [CrossRef]

92. Molodkina, E.; Danilov, A.; Feliu, J.M. Cu UPD at Pt (100) and stepped faces Pt (610), Pt (410) of platinum single crystal electrodes. *Russ. J. Electrochem.* **2016**, *52*, 890–900. [CrossRef]

93. Markovic, N.; Ross, P. Effect of anions on the underpotential deposition of copper on platinum (111) and platinum (100) surfaces. *Langmuir* **1993**, *9*, 580–590. [CrossRef]

94. Fiçicioğlu, F.; Kadirgan, F. Characterization of a Pt+ Pd alloy electrode by underpotential deposition of copper. *J. Electroanal. Chem.* **1993**, *346*, 187–196. [CrossRef]

95. Solla-Gullón, J.; Vidal-Iglesias, F.; Herrero, E.; Feliu, J.; Aldaz, A. CO monolayer oxidation on semi-spherical and preferentially oriented (1 0 0) and (1 1 1) platinum nanoparticles. *Electrochem. Commun.* **2006**, *8*, 189–194. [CrossRef]

96. Solla-Gullón, J.; Rodríguez, P.; Herrero, E.; Aldaz, A.; Feliu, J.M. Surface characterization of platinum electrodes. *Phys. Chem. Chem. Phys.* **2008**, *10*, 1359–1373. [CrossRef]

97. Coutanceau, C.; Urchaga, P.; Baranton, S. Diffusion of adsorbed CO on platinum (100) and (111) oriented nanosurfaces. *Electrochem. Commun.* **2012**, *22*, 109–112. [CrossRef]

98. Solla-Gullón, J.; Vidal-Iglesias, F.; Rodriguez, P.; Herrero, E.; Feliu, J.; Clavilier, J.; Aldaz, A. In situ surface characterization of preferentially oriented platinum nanoparticles by using electrochemical structure sensitive adsorption reactions. *J. Phys. Chem. B* **2004**, *108*, 13573–13575. [CrossRef]

99. Chierchie, T.; Mayer, C.; Lorenz, W. Structural changes of surface oxide layers on palladium. *J. Electroanal. Chem.* **1982**, *135*, 211–220. [CrossRef]

100. Chierchie, T.; Mayer, C. Voltammetric study of the underpotential deposition of copper on polycrystalline and single crystal palladium surfaces. *Electrochim. Acta* **1988**, *33*, 341–345. [CrossRef]